# Liquid/liquid interface synthesis of poly (5-aminoindole) and its Langmuir assisted self-assembly at air-water interface

## 4.1 Introduction

Environmental stability, better solution processability, low production cost with better electrochemical and electronic properties of CPs are the major advantages that gain great attention in electronic industry [6,7]. Based on these properties, few polymers have recently been enforced as semiconducting layer in diodes, field effect transistors, photovoltaic devices, chemical and biosensors [2,8,9,70,72]. The performance of any such device is very much affected by the molecular orientation along charge transportation direction. In the past few decades, major attention has been drawn towards their semiconducting layer alignment and processing conditions for enhancement in the device electrical properties by opting the appropriate synthetic and fabricating route [2,6-8]. Their soft and fragile nature has opened the door to solution based fabrication methods such as spin coating, spray coating, LB, etc. amongst which the LB technique is worth citing that employs mobile liquid substrate for molecular level ordering of the polymeric materials [53,54,56,57].  Mainly, ordering from solution route is desired because of various advantages associated such as (1) ample opportunity for self-assembly in solution phase via secondary interactions, (2) ease of transferring assembled polymers onto substrates of choice, (3) mobile subphase in some cases such as LB and FFTM technique facilitating large scale, ordered self-assembly of (soft) polymers. Langmuir technique undoubtedly provides an excellent platform for molecular level ordering of the solution processable molecules to assemble [53,54]. This technique is substantially preferred for less solution processable materials (that sparsely disperse into solution). Unlike other techniques that offer solid substrate for molecular orientation, this technique aids in

uniform film formation over large area on liquid subphase at air-water interface with molecular level ordering [53,54]. Here we would like to emphasize on the pre-fabrication step i.e. synthetic route to control ordering of the polymer chains at the initial level and the fabrication step i.e. ordering of polymers during film formation. Prior to film processing, synthetic route employed for polymerization has a great significance on the polymer morphology and its properties as supported by literature [35,72,86]. Chemical and electrochemical polymerization techniques are the two well known used methods to synthesize conducting polymers. However, chemical synthesis of polymers got much more attention in the recent past as it circumvents the problem of requirement of materials in bulk and post-synthesis modifications and composites formation [2,6-8]. Still, control of morphology, processability and chain ordering (crystallization) are the major issues in chemical synthesis. Therefore, processable ordered polymers film synthesis has become a keen area of research interest in the recent years. To address these issues in-situ polymerization with template techniques and interfacial synthesis displayed much more advantages over conventional synthesis techniques [6,44,72,77]. However, template techniques employ templates (hard and soft), which is a major disadvantage, as they need to be removed to obtain a pristine polymer. The well-known techniques that avoid the use of a template are electrochemical or micelles based chemical synthesis otherwise post synthesis ordering and self assemblies are possible by LB-film casting, electron beam lithography, electro-spinning, etc. [2,35,44,53,57]. The electrochemical synthesis of conducting polymers has also been of interest for a number of years and is successfully demonstrated for varieties of monomers [7,70,86]. However, due to low yield and loss in redox property after deposition on electrodes during polymerization process (over potential), chemical synthesis is preferable. Moreover, control of morphology and composite formation are other major attractions for use of chemical synthesis for CPs.

Herein, we are interested in bulk and processable ordered polymer film synthesis, so interfacial polymerization technique unveiled the potential to address the issues related to the conventional or template chemical synthesis [47-49]. For this purpose, two immiscible solvents are employed containing two chemically reactive species (forming two phases) respectively, and polymerization occurs at the interface. Interfacial polymerization permits finite side reactions (and byproducts) as it is a step process and evades the requirement of any phase transfer agents or catalysts. It can be proficiently carried out in one pot with different immiscible solvent pairs and varying reagent concentrations. CPs with heteroatoms in the monomer unit result in a stable structure due to the lone pair of electrons of the heteroatoms that participate in $\pi$-electron conjugation [7,107]. However, among various N-containing conducting polymers, PIn and its derivatives have not been scrutinized much due to their lower polymerization efficiency and the conductivity [87,108-110]. This is probably due to variety of polymerization schemes employed till now. So, there is a need of synthesis technique that can yield regioselective structures leading to lower deviation from planarity. We have tried to deal with this issue to some extent in our work.

Polymers of this family have drawn keen attention for the sake of their good thermal stability, high redox activity, electrocatalytic properties, charge transport properties, electrochromic properties and above these, no toxicity [87,108-110]. Here, we have chosen an amino derivative heteroaromatic monomer "5-AIn", to synthesize 5-APIn. The influence of amino substituent and heteroatom in the ring on the physical and chemical properties of the polymeric product has been investigated. As per available reports, 5-APIn has been well synthesized by electrochemical method, but there is no report available on chemical synthesis of this polymer to the best of our knowledge

[86,87,89]. Therefore, we report here, an interfacial chemical polymerization of 5-APIn without the aid of any template at room temperature (25 ± 1 °C). Further, the as-synthesized material has been used for the modification of commercial Au-electrode in order to explore its better redox behavior compared to 5-APIn synthesized by other method. Also, band gap calculated via UV-Vis spectroscopy and CV were compared with electronic band gap obtained via DFT calculations. These variant properties motivated us to explore its large area, uniform film formation for electronic device applications. However, its poor solubility in common organic solvents, prompted us to exploit Langmuir technique that necessitates the dilute dispersion of material for spreading onto water subphase rather than other fabricating methods [53,54]. Further its film fabrication was done via LS method. This work highlights the importance of mobile aqueous subphase of Langmuir method that is offering an opportunity for ordering and self-assembly of 5-APIn thus removing its impedance for application in large area electronic device applications.

## 4.2 Results and discussion

### 4.2.1 Molecular Studies of 5-APIn

The chemical synthesis of 5-APIn is of significant interest due to low polymerization efficiency via other techniques like electrochemical technique [87,89]. In addition to its bulk yield, the interfacial technique was deliberately opted to control the ordering of polymer at the interface. Synthesis protocol has been discussed in chapter 2 section 2.2.4. Here, the oxidative coupling of 5-AIn was initiated via protonation of the amino group that exerts electron withdrawing effect to accelerate the reaction [112]. A dark reddish brown solid at the aqueous/organic interface was suspended at the final stage of reaction due to protonated amino group (as shown in Figure 2.3). Tentative polymerization

mechanism affects the linkage of monomers in polyindole backbone. Mainly two linkages have been reported for pyrrole unit of PIn like 1, 3 or 2, 3-positions that bear conjugating unit (-N-CH=CH-)$_n$ for 1, 3-linkage involving N atom and (-CH=CH-)$_n$ for 2, 3-linkage polymerization [73,113]. Therefore, the existence of N-H needs to be verified to conclude the type of linkage in PIn and its derivatives. Though FT-IR can resolve the debating existence of N-H bond, the trapped moisture may disrupt the peak positions [114]. So, we considered ^{1}H-NMR spectroscopy as more accessible and pronounced technique for the verification of N-H bond existence [113].
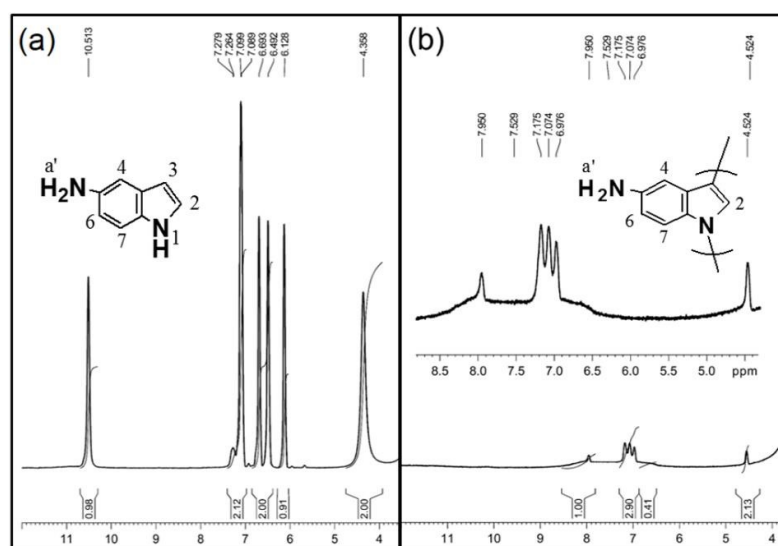


**Figure 4.1** ^{1}H-NMR spectra of (a) 5-AIn (b) 5-APIn

**Table 4.1** Proton chemical shifts (δ) of 5-AIn and 5-APIn.

| δ (ppm) | H-1 | H-2 | H-3 | H-4 | H-6 | H-7 | a' |
|---------|-----|-----|-----|-----|-----|-----|-----|
| 5-AIn | 10.5 | 6.49 | 6.12 | 7.26-7.27 | 6.69 | 7.08-7.09 | 4.35 |
| 5-APIn | - | 6.89 | - | 7.95 | 7.07 | 7.17 | 4.52 |

Usually, N-H of pyrrole appears around 8 ppm, but due to increase in conjugation, proton chemical shift (δ-value) in indole moved towards the lower field (10.5 ppm) as shown in Figure 4.1(a). On comparing ^{1}H-NMR spectra of 5-AIn and 5-APIn (as shown in Table

4.1) downfield shift in δ-values in the case of polymer was observed due to its larger extent of conjugation compared to the monomer. The chemical shift for pyrrolic N-H bond in 5-AIn is absent for 5-APIn, which confirmed the linkage through N-atom of the pyrrole ring of 5-AIn during polymerization [115,116]. The monomer, 5-AIn exhibited five peaks in the aromatic region representing the aromatic protons of benzene and pyrrole, which reduced to four in 5-APIn and a shift towards higher d-values was observed due to enhanced delocalization of pelectrons. The corresponding peak for H-3 is missing in the case of 5-APIn indicating the involvement of C-3 in polymerization. Amino (-NH$_2$) group of 5-AIn at C-5 can be seen in the ^{1}H-NMR spectrum of 5-APIn at 4.52 ppm that confirmed its retention in the polymer backbone as a pendant group. Thus, it explained the polymerization of 5-APIn via 1, 3-linkage of monomer unit with retention of -NH$_2$ group at C-5 [112-116]. The structural information of 5-APIn was characterized further and compared with 5-AIn using FT-IR analysis (as shown in Figure 4.2 and Table 4.2) with the supportive inclusion of earlier reports [112,113, 117].

On the basis of these reports, two main controversial opinions on the linkage (as explained above) of PIn and its derivatives prepared chemically, is resolved herein. The polymerization mechanism includes intra- and inter-chain interactions (hydrogen bonding and π-π interactions) that are affected by the type of dopant and nature of the solvent employed during the process [117].

These interactions, as well as the introduction of an amino substituent at C-5, altered the vibrational parameters of 5-AIn as compared with indole molecule [118]. Polymerization mechanisms in polyindoles are usually assured by the existence of N-H stretching or bending mode in the spectrum [115,116].

In 5-AIn, N-H stretching vibration of the 2° amine of pyrrole unit moved towards lower
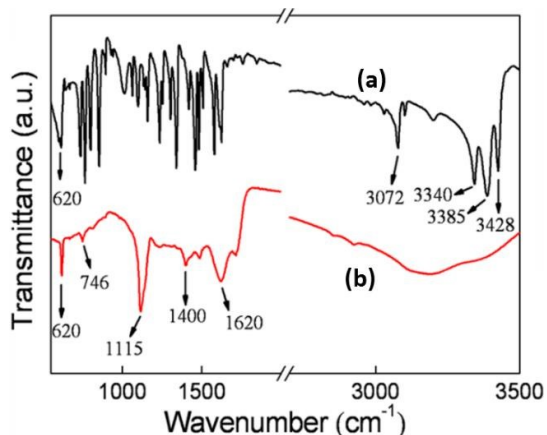
**Figure 4.2** FT-IR spectra of (a) 5-AIn (b) 5-APIn.

**Table 4.2** FT-IR band assignment of 5-AIn and 5-APIn.

| S. No. | Band assignment | Vibration frequency (cm$^{-1}$) | |
|:---:|---|:---:|:---:|
| | | **5-AIn** | **5-APIn** |
| 1. | N-H stretching | 3385 | - |
| 2. | NH$_2$ (asymmetric and symmetric stretching) | 3428, 3340 | 3190 |
| 3. | N-H bending (NH$_2$ scissoring) | 1576 | 1620 |
| 4. | C-H bending (in-plane) | 1348 | 1400 |
| 5. | C-C stretching | 1600-1400 | 1600-1400 |
| 6. | C-N stretching | 1156 | 1115 |
| 7. | C-H (in-plane) deformation (benzene ring hydrogens) | 765 | 746 |
| 8. | NH$_2$ bending (out of plane / wagging) | 620 | 620 |

frequency, i.e. 3385 cm$^{-1}$ due to NH-$\pi$ hydrogen bonding [117]. NH$_2$ group displayed asymmetric and symmetric stretching at 3428 and 3340 cm$^{-1}$ respectively [115-118]. Overtone due to N-H bending overlapped with the N-H symmetric stretching mode and a peak at 3072 cm$^{-1}$ was observed for aromatic C-H stretching. The peaks as mentioned above altogether resembled a broad band near 3190 cm$^{-1}$ in 5-APIn indicating the retention of NH$_2$ pendant group (as verified above in 1H NMR spectrum). The peak at

1620 cm$^{-1}$ in 5-APIn attributed to the NH$_2$ scissoring vibration (N-H bending). It means that NH$_2$ group persists in the polymer main chain and is not involved in polymerization. This is in well accordance with the ^{1}H-NMR results as explained above. C-H in-plane bending at 1348 cm$^{-1}$ and C-C stretching modes in the range of 1600-1400 cm$^{-1}$ of the benzene ring observed in 5-AIn were persistent in 5-APIn. The peak at 1115 cm$^{-1}$ is attributed to the C-N stretching mode. Peak at 746 cm$^{-1}$ in 5-AIn is persistent in 5-APIn (765 cm$^{-1}$) corresponding to C-H deformations (in-plane bending) of benzene ring hydrogens. This further suggested the involvement of pyrrole ring as the polymerization site rather than benzene ring [113,118]. Peak at 620 cm$^{-1}$ indicates the out of plane bending for NH$_2$ (wagging mode) further confirming the existence of amino substituent at C-5 of 5-APIn [117].

Thus, ^{1}H-NMR together with FT-IR spectra supported our hypothesis of 1, 3- linkage in 5-APIn. Based on this, a plausible polymerization mechanism of 5-AIn has been proposed (Figure 4.3) which is closely similar to earlier reports [115,116]. As per earlier reports, it is evident that substituent present especially at C-5 position of indole plays a crucial role for the fusion of monomers [111,112,115]. For example, electron donating groups (EDG) at C-5 stabilize the indole radical cation intermediate and thus reduce the rate of polymerization. Similarly, electron withdrawing groups at C-5 enhance the spin density at N-1 and C-3 only of five-membered ring radical cations as the probability of loss in aromaticity of benzene ring renders its participation in the linkage [112].

In our work, we have proved 1, 3-linkage in 5-APIn via ^{1}H-NMR and FT-IR spectra considering the electron withdrawing nature of protonated amino group (-NH$_3^+$). In order to estimate the electronic properties of the assynthesized polymer, we carried out significant experimental and computational efforts. We, approximately calculated band
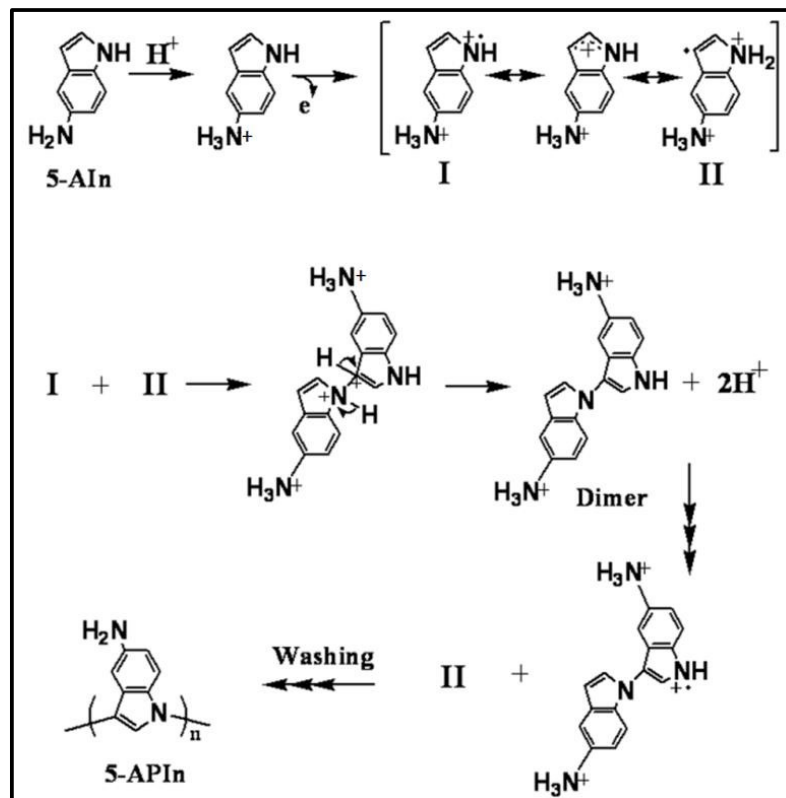
**Figure 4.3** Plausible mechanism of polymerization of 5-AIn.

gap via UV-Vis spectroscopy ($E_g$), cyclic voltammetry ($E_{cv}$) and theoretically via range-separated density functionals ($\Delta E$).

Optical properties of 5-APIn were investigated and compared with 5-AIn using UV-Vis absorption spectroscopy in DMSO solvent at room temperature. As illustrated from these absorption spectra, 5-AIn featured two absorption peaks at 274 nm and 321 nm corresponding to $\pi$- $\pi^*$ and n- $\pi^*$ transitions respectively (as shown in Figure 4.4 (a)). However, these peaks shifted towards longer wavelength to 281 nm and 328 nm in the case of 5-APIn confirming larger extent of conjugation. A broad hump in the region of 400-550 nm (polaronic band formation) was observed indicating the delocalization of charges on polymer backbone [47,72,80,119]. The optical band gap of 5-APIn was computed on the basis of direct allowed transition in absorption spectra. It was figured
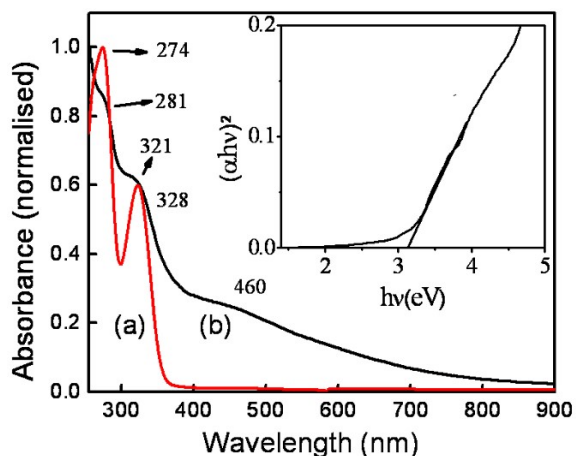
**Figure 4.4** UV-visible spectrum of (a) 5-AIn (b) 5-APIn (Inset shows optical band gap of 5-APIn).

using the fundamental expression of Taucs' plot as in Equation (4.1),

$$\alpha h\mathcal{V} = B(h\mathcal{V} - E_g)^n \qquad (4.1)$$

where a, hn and B symbolize absorption coefficient, energy of absorbed light (incident photon energy), proportionality constant respectively and n=1/2 for direct allowed transition [119]. Optical band gap ($E_g$) of 5-APIn was determined as 3.06 eV by plotting a graph of $(\alpha h\mathcal{V})^2$ versus $h\mathcal{V}$ (as shown in inset of Figure 4.4), and then extrapolating the linear part of the curve towards abscissa (zero) [80,119].

Number average molecular weight (Mn) and weight average molecular weight (Mw) of 5-APIn were determined using Gel Permeation Chromatography (as shown in Figure 4.5). Multiple peaks with minuscule humps were observed for 5-APIn which revealed the occurrence of polymeric chain fragments. This suggests wide range distribution of Mn with low molecular weight polymeric fragments [120]. Polydispersity index (PDI) was calculated as 1.09 [Mw (7200)/Mn (6600)] (Remark: We are assuming here that undissolved particles are eluted first and can be seen corresponding to small peak 1. So, it may be ignored).
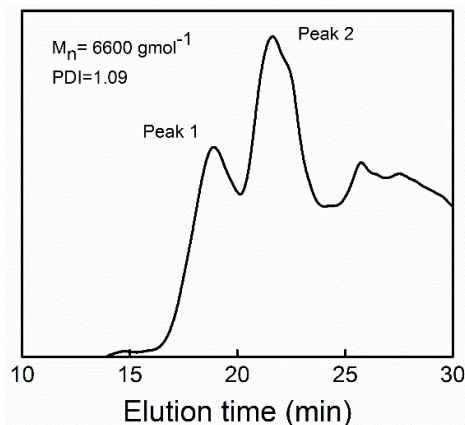
**Figure 4.5** Gel permeation chromatogram of 5-APIn.

XRD pattern of as-synthesized 5-APIn (as shown in Figure 4.6) depicted that 5-APIn shows broad hump centered at $2\theta=25°$ with two well known characteristic peaks at $2\theta=19.8°$ and $25.9°$ similar to PIn [119]. Apart from this, there are additional small peaks observed at $2\theta=16.9°$, $27.2°$, $30.2°$ and $32.4°$. This revealed better organization of chains indicating higher number of crystallite zones than the unsubstituted PIn or other derivatives of PIn reported earlier [69,72,80]. This observance accounts to the presence of better alignment of a different fractional range of oligomer units in polymer backbone. The initially formed film acts as a pseudo template for further polymerization at interface of two solvents resulting in better alignment.
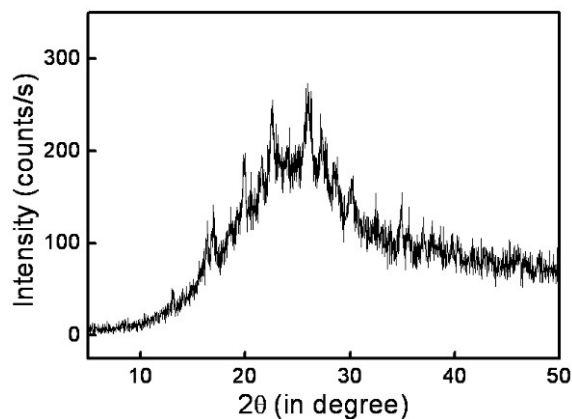


**Figure 4.6** XRD pattern of 5-APIn.

## 4.2.2  Surface morphology studies

Surface morphology of as-synthesized 5-APIn with respect to growth time was analyzed
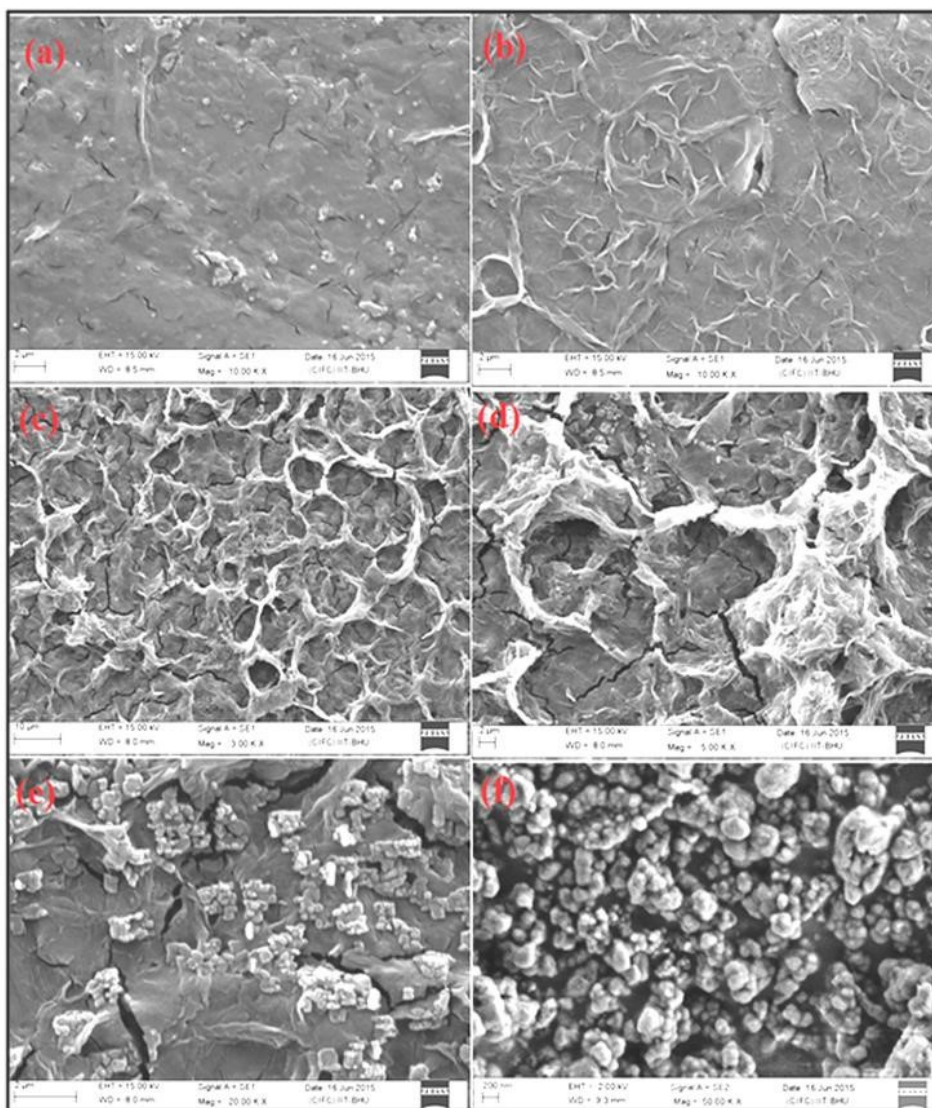


**Figure 4.7** SEM images of 5-APIn formed at the interface after (a) 3 min, (b) 5 min, (c) 15 min, (d) magnified form of image (c), (e) 60 min and (f) after 24h.

by SEM as shown in Figure 4.7 (a-f). Images of as-grown material at different time intervals from the interface were examined at carbon stab. We observed that nucleation in material started at 3 min after addition of APS (Figure 4.7 (a)) that grew into flake type

structure at 5 min (Figure 4.7 (b)). Then after, these flakes curled into its bigger form at 15 min (Figure 4.7 (c) and (d)) and bigger flakes with small globules at 60 min (Figure 4.7 (e)). Finally, these flakes disappeared at 24 h leaving behind small globules of the random size distribution (Figure 4.7 (f)). It is due to unstable micelles formation at the interface (no stabilizer is used) that resulted in porous and non-uniform globular morphology (at 24 h) for polymers undisturbed for a longer period [72]. This type of morphology generates larger surface area for electrochemical chemical reaction [88,121]. Based on this observation, the concept of constant phase element was procured due to inhomogeneous charge distribution over polymer matrix (discussed later in EIS results).

### 4.2.3   Thermal studies

Thermal stability of 5-AIn and 5-APIn was investigated by thermogravimetric analysis that is a noteworthy way of studying thermal degradation behavior. The result obtained was similar to the PIn family reported previously [87,108,109,110]. An endothermic peak around 132 °C in DTA curve of 5-AIn signified the first weight loss region due to the removal of physically adsorbed water molecules (Figure 4.8 (a')). Decomposition of monomer started around 276 °C (Figure 4.8 (a)), which exhibited maximum weight loss (TGA curve). Figure 4.8 (b & b') displayed two-step weight loss behavior for the 5- APIn that was depicted by two slope changes. An initial weight loss of 10% from room temperature to 100 °C on TGA curve (Figure 4.8 (b)) was observed probably due to desorption of water. Another slope change was observed in the range of 200-300 °C (5%) signifying the degradation of the polymer chain (Figure 4.8 (b & b')). Overall, 5-APIn resembled less percentage weight loss (40%) up to 600 °C than the monomer, which was degraded almost completely. This result indicated better thermal stability of 5-APIn.
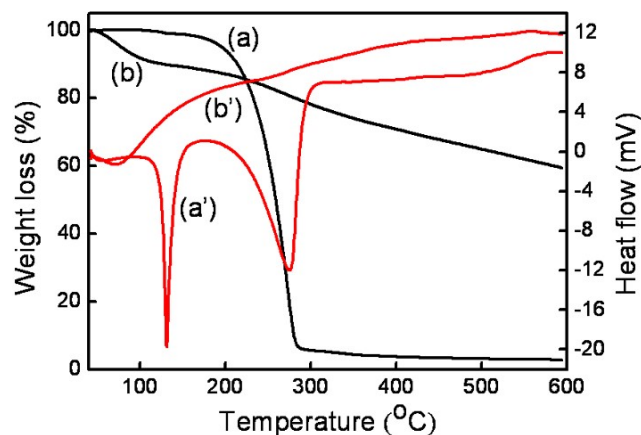
**Figure 4.8** TGA and DTA curves of 5-AIn (a & a') and 5-APIn (b & b') respectively.

## 4.2.4 Electrochemical studies

As reported in literature, same polymer synthesized electrochemically undergoes irreversible degradation on application of oxidizing potentials greater than 0.6 V [87,88,122]. This phenomena of loss in electrochromic properties at potentials greater than 0.6 V is due to over-oxidation [87,88]. However, our employed technique yielded polymer unveiling the retention of excellent electroactivity even at higher positive potentials described below. Redox properties of the 5-APIn modified Au electrode (5-APIn/Au) were analyzed with the aid of CV. Electrode fabrication is already explained in experimental section. Cyclic voltammogram of the 5- APIn/Au and bare Au electrode were obtained in 0.1 M TBAP (dissolved in DCM) as supporting electrolyte (scan rate of 50 mV/s) in the potential window of -1.1 V to 1.1 V (as shown in Figure 4.9). The 5-APIn displayed well-defined redox behavior with oxidation peak at 0.96 V and reduction peak at -0.96 V along with a new peak at 0.44 V (as shown in inset of Figure 4.9) vs. Ag/Ag$^+$. This newpeak is due to redox quasi-reversibility of 5-APIn (as discussed later) [123,124]. Herein, presence of -NH$_2$ and protonated amine groups as well as conjugation in the polymer backbone allows it to be doped. Thus, 5-APIn showing 1,3-linkage behaves as an n-doped as well as p-doped semiconducting material (depicted from the
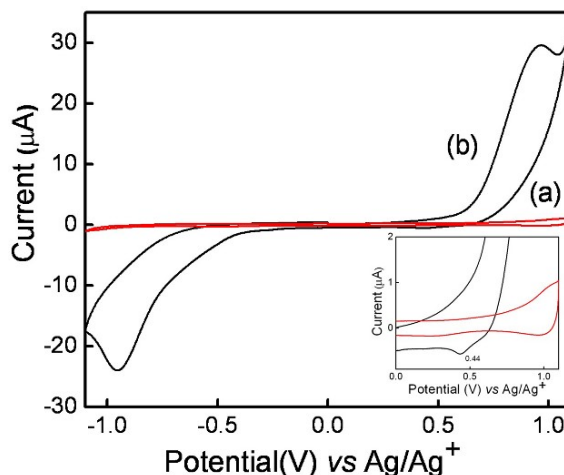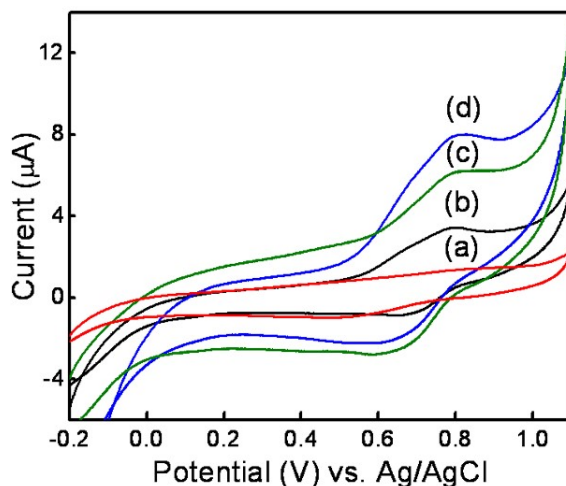
**Figure 4.9** CV of (a) bare Au electrode (b) 5-APIn/Au. The inset shows an enlarged view of similar CV plot.

result) with an electrochemical band gap ($E_{cv}$) of 3.07 eV [123].

CV was also recorded in 0.5 M $H_2SO_4$ solution as supporting electrolyte at different scan rates (20, 50, 100 mV/s) from -0.2 V to 1.1 V to further check the electroactivity of 5-APIn/ Au (as shown in Figure 4.10). It is worth mentioning here, that we were unable to scan successfully towards more negative potentials like former case due to hydrogen evolution [86,87,124]. 5-APIn exhibited redox quasi-reversibility at 0.81 V and 0.63 V vs. Ag/AgCl corresponding to state I and state II as proposed in Figure 4.11 where redox transformation proceeds with the exchange of $H_3O^+$ ions [70,86]. However, on comparing the electroactivity of the 5-APIn/Au observed in $CH_2Cl_2$/TBAP and 0.5 M $H_2SO_4$ electrolytes, the electroactivity obtained in latter case is lower (with low redox current) than the former case. This is due to different interactive behavior of the polymer with the electrolytes and involvement of ion exchange via $H_3O^+$ ions (responsible for the change in pH) [70,86]. As we are expecting that polymer backbone may contain hybrid of -$NH_2$ and protonated amine groups at the same time. These functionalities act as electron donating and electron-withdrawing group respectively leading to the formation of

electron-rich and electron deficient conjugated backbone. Thus, this material is flooring its way towards n-type and p-type electrical conductors. We also observed a slight change in the peak potentials on varying scan rates in aqueous electrolyte. This reveals the redox recyclability of 5-APIn between proposed state I to state II without any significant decomposition with the diffusion-controlled process [70,86].



**Figure 4.10** CV of (a) bare Au electrode and 5-APIn/Au in presence of 0.5 M $H_2SO_4$ at scan rate (b) 20 $mVs^{-1}$, (c) 50 $mVs^{-1}$ and (d) 100 mV $s^{-1}$.

This behavior is also verified by EIS as explained later. Taken together, we observed consistent quasi-reversible redox behavior of the waves even at positive potentials (>0.6 V) unlike that observed for electrochemically synthesized 5-APIn [86,87,122]. Thus, we can say that our methodology yielded an excellent electroactive polymer.

EIS was carried out to study the inhomogeneous charge distribution over polymer matrix due to non-uniform globular morphology (as observed in SEM results). It also complimented the redox recyclability of 5-APIn observed (refer to Figure 4.10 and Figure 4.11) without any significant decomposition with the diffusion-controlled process. EIS study expressed the involvement of internal resistances acting between the reference

electrode and working electrode during electrochemical phenomenon. The current flow

by applying a voltage
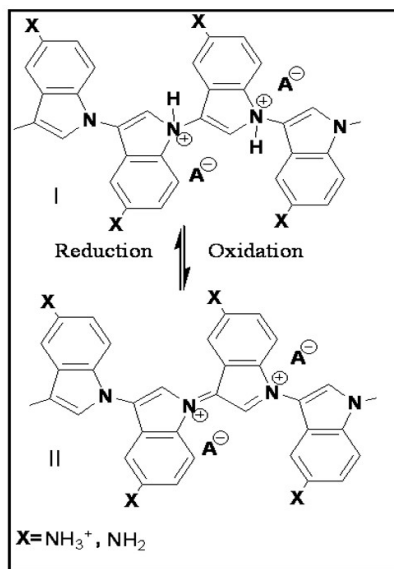


**Figure 4.11** Schematic representation of redox recyclability behavior of 5-APIn in 0.5M

$H_2SO_4$.

at a set frequency was recorded by the potentiostat and converted into an impedance value

(real (Z'); imaginary component (Z")) via software. This was studied in terms of Nyquist

plot for 5-APIn/Au electrode as shown in Figure 4.12. In the electrochemical experiment,

combination of various elements such as solution resistance ($R_s$), constant phase element

(Q or CPE), charge transfer resistance ($R_{ct}$) and the Warburg element (W) contributed to

the total impedance of the system which is represented in the form of Randles circuit

[125]. CPE was observed due to charge accumulation over the inhomogeneous surface

(as inferred from SEM images).W accounts for the diffusion controlled process that is

observed at regions (or high -Z"). The high-frequency (or low -Z") region represents

opposition offered to electron movement known as resistance to charge transfer ($R_{ct}$). It

can be seen that straight line part of 5-APIn/ Au electrode shows a higher inclination
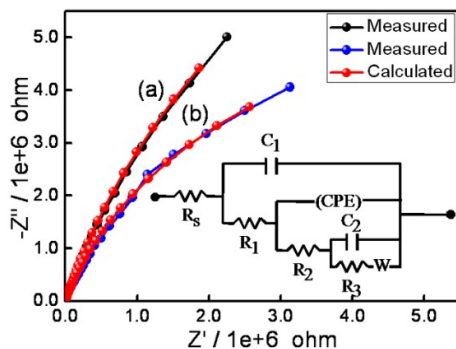
**Figure 4.12** EIS of (a) bare Au electrode, (b) 5-APIn/Au. (inset: EIS data fitted by ZSimp software for bare Au electrode and 5-APIn/Au with their electrical equivalent circuit.)

**Table 4.3** EIS parameters calculated from the equivalent circuit model.

| Material | $R_s$ ($\Omega$) | $C_1$ ($\mu F$) | $R_1$ ($\Omega$) | CPE ($\mu S.s^n$) | Freque ncy power ($0<n<1$) | $R_2$ ($\Omega$) | $C_2$ ($\mu F$) | $R_3$ ($\Omega$) | W ($S.s^{1/2}$) |
|---|---|---|---|---|---|---|---|---|---|
| 5-APIn/Au | $10^{-2}$ | $4.76 \times 10^{-3}$ | 1658 | $1.35 \times 10^{-6}$ | 0.7997 | 519.5 | 0.3 | $1.33 \times 10^7$ | $2.92 \times 10^5$ |
| Bare Au electrode | $10^{-2}$ | $10.47 \times 10^{-3}$ | 1597 | $1.67 \times 10^{-6}$ | 0.8421 | $1.654 \times 10^5$ | 0.13 | $2.83 \times 10^7$ | 115.7 |
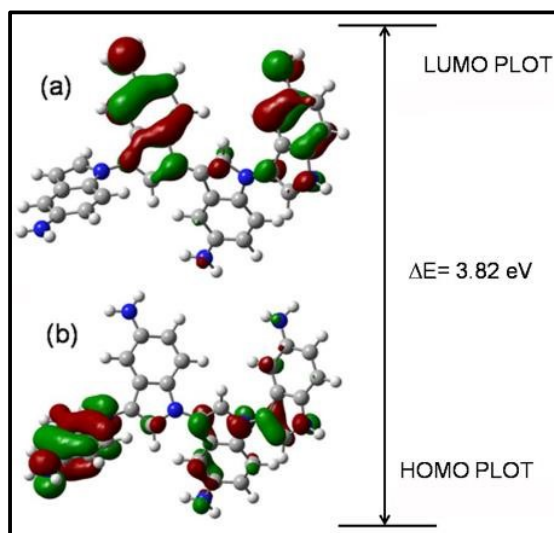


**Figure 4.13** Electron distribution for the 5-APIn (a) HOMO and (b) LUMO energy levels obtained at the wB97XD/6-31G* level of theory in gas phase. Here blue, gray and white balls represent N, C and H-atoms respectively.

towards the -Z" axis at low-frequency side depicting the diffusion controlled process due to higher charge accumulation near the electrode surface [110].

## 4.2.5 Theoretical studies

Density functional theory (DFT) calculations were performed to predict reasonable structure and electronic properties of the assynthesized polymer. Computational studies on PIn have already been performed earlier in order to study the polymerization mechanism mainly via 2,3-linkage [126]. However, in the present work, we have tailored the electronic band gap of a 5-substituted polymer (5-APIn) containing 1,3-linkage. We have employed the hybrid functional instead of conventional functional, as it overcomes the problems associated with chain-length dependence of band gaps for conducting organic polymers. To the best of our knowledge, most suitable functional among range-separated hybrids for oligomers with 3-8 rings is wB97XD [127].So, theoretical band gap was computed with the wB97XD functional along with 6-31G* basis set for the 5-APIn [126,127]. Four 5-AIn molecules are decorated in the most appropriate spatial arrangement of atoms/ groups, and defects were intentionally created at two electron-rich centers (N-atom) in order to show the conducting behavior of 5- APIn. Geometry of 5-APIn was fully optimized in gas phase. A benefit of hybrid functionals is that they estimate gas-phase DFT HOMO-LUMO gaps for polymer that are very close to $E_g$ and $E_{CV}$ values produced experimentally [127]. In order to ensure the minima on the potential energy surface vibrational frequency analysis was also carried out at the same level of theory and all frequencies were found to be real. Inclusion of defects in the molecular backbone of 5-APIn leads to the distortion in co-planarity that ultimately inhibits electronic conduction to some extent.

Frontier molecular orbital (FMO) calculations were also performed at the wB97XD/6-

31G* level of theory in gas phase in order to get the insights about the theoretical band gaps. Molecular orbital diagram is obtained by generating the molecular orbitals by population analysis with isovalue 0.03 using Gauss View. Highest occupied molecular orbital (HOMO) and the lowest unoccupied molecular orbital (LUMO) are collectively known as frontier molecular orbitals as they form the outermost boundaries of the electrons of the system. It is clear from Figure 4.13 that HOMO is localized over 1st and 3rd monomer unit of the polymer (tetramer) and LUMO is localized over 2nd and 4th unit of the polymer (tetramer). The difference (DE) between HOMO and LUMOwas calculated to be 3.82 eV. Overall, the theoretical band gap (DE) agree qualitatively well with the optical band gap, Eg (3.06 eV) and electrochemical band gap, Ecv (3.07 eV) obtained experimentally. All the calculations were performed using Gaussian 09 program and HOMO LUMO are plotted with Gauss-View [128].

## 4.2.6   Isotherm studies

Stable dispersion of 5-APIn in DMSO:chloroform (1:10) was spread on mobile water surface to study its $\pi$-A isotherm at 25 °C (as shown in Figure 4.14). The $\pi$-A isotherm
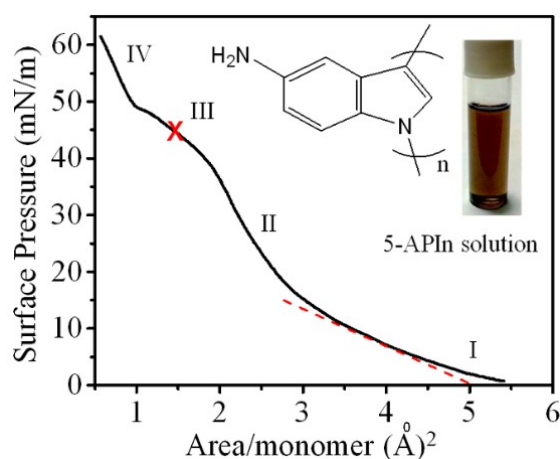


**Figure 4.14** Pressure-area ($\pi$-A) isotherm of 5-APIn depicting various regions I, II, III, IV (inset shows 5-APIn dispersion)

provides useful information about the intermolecular interaction as well as film stability at air-water interface. 5-APIn solution (dispersion) when spread onto water subphase, molecules orient themselves at the air-water interface to minimize their free energy. This material when compressed (compression speed=10 mm/min) slowly, affects the surface pressure (differential surface tension, $\pi = \gamma_{o\ (water)} - \gamma_{(material)}$). Pseudomonolayer (in this case) formed undergoes various phase transformations corresponding to three dimensional gases, liquids and solids. These phase changes are then recognized by observing the surface pressure ($\pi$) as a function of the area covered by the pseudomonolayer film [53,54].

Figure 4.14 presents four distinct areas namely region I accounting to widely spread molecules (similar to gas phase), region II describing liquid phase, region III representing condensed liquid phase, and region IV depicting solid phase [18,55,76]. Region III (liquid condensed phase) is the nearly plateau area where molecules are supposed to be just close enough to form uniform compact film. This observation is supported by the SEM results discussed later. The Langmuir floating films were lifted at the curve mid-point (45 mN/m) in a horizontal fashion (Schaefer style) so as to prevent the disruption in uniformity of rigid monolayer unlike observed during vertical lifting of non-alkyl chain polymers [53-55,76]. Langmuir films of various non-amphiphilic compounds or polymers reported are usually rigid and undergo breakage of films during vertical lifting. Therefore, LS method employing horizontal lifting is much preferred for its fabrication [55,76].

### 4.2.7 Film microscopic studies

SEM micrographs of 5-APIn LS films, lifted horizontally at different surface pressures (35, 45 and 55 mN/m) are shown in Figure 4.15 (a-e). Figure 4.15 (a) (at 35 mN/m) depicts non-uniform film containing gaps, (b) (at 45 mN/m) smooth and uniform film,

(c) its magnified image depicting few cracks, (d) (at 55 mN/m) folded film, and (e) multilayer (5L) LS film lifted at 45 mN/m for measuring electrical parameters discussed later. At 35 mN/m SP, the molecules start coming closer but are left with some gaps that diminish with increasing SP (i.e. at 45 mN/m). On further compressing the barriers (55 mN/m) the film starts folding and layers overlap each other [18,55,76]. These observations clearly validate 45 mN/m pressure as the optimum one for proceeding towards compact and uniform film deposition.

AFM (2D and 3D) images of the as deposited 5-APIn LS at 45 mN/m were obtained as shown in Figure 4.16. It clearly depicts the uniformly decorated globular 5-APIn structures with compact arrangement [51,55,76]. Horizontal and vertical surface profiling (Figure 4.16 c & d) was also done via Nova software to examine the uniformity in both x and y direction of the LS film. The inset profile graph in both cases depict the maximum 20 nm roughness over the large area of 8 x 8 $\mu m^2$ area. The root mean square (rms) roughness value of 4.495 nm and roughness average of 3.446 nm also assures the large area surface uniformity [55,63,76].

## 4.2.8 Film spectroscopic studies

Raman spectroscopy has been done to investigate the ordering and assembly of 5-APIn via LS method in comparison to that of bulk polymer (as shown in Figure 4.17). Bulk 5-APIn (powder) displays two broad major peaks at 1332 (pyrrole ring stretch of indole) and 1554 cm$^{-1}$ (benzene ring stretch of indole) (Figure 4.17 (a)) characteristic of polyindole family [18,55,82,118]. Whereas, 5-APIn LS film revealed multiple peaks at 535, 578, 1082, 1328, 1401 and 1563 cm$^{-1}$. The spectra clearly demonstrates the significant shift of major peaks (1332 and 1554 cm$^{-1}$) towards higher wave number
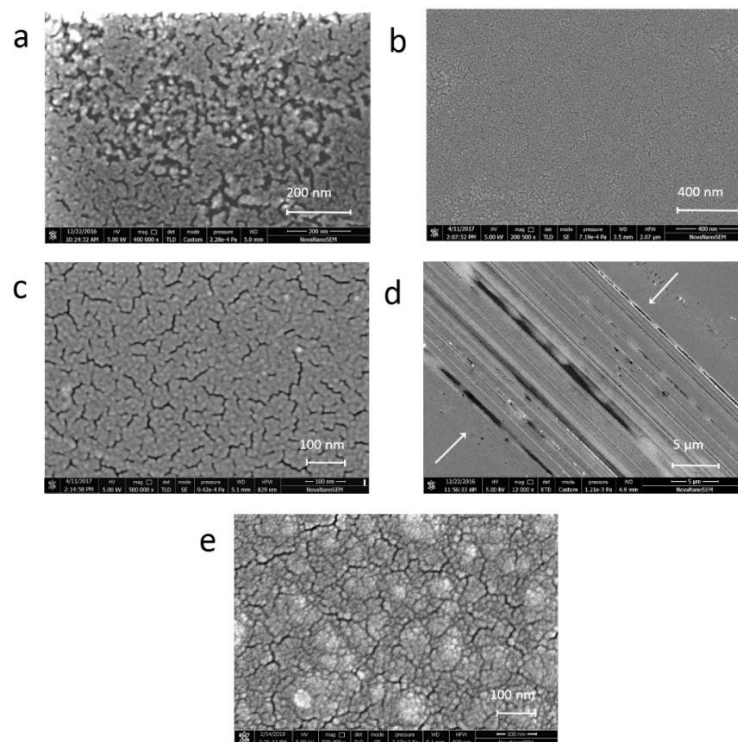
**Figure 4.15** SEM images 5-APIn LS film deposited at different pressures (a) 35, (b) 45, (c) magnified image of b, (d) 55 mN/m, and (e) multilayer (5L) LS film lifted at 45 mN/m.
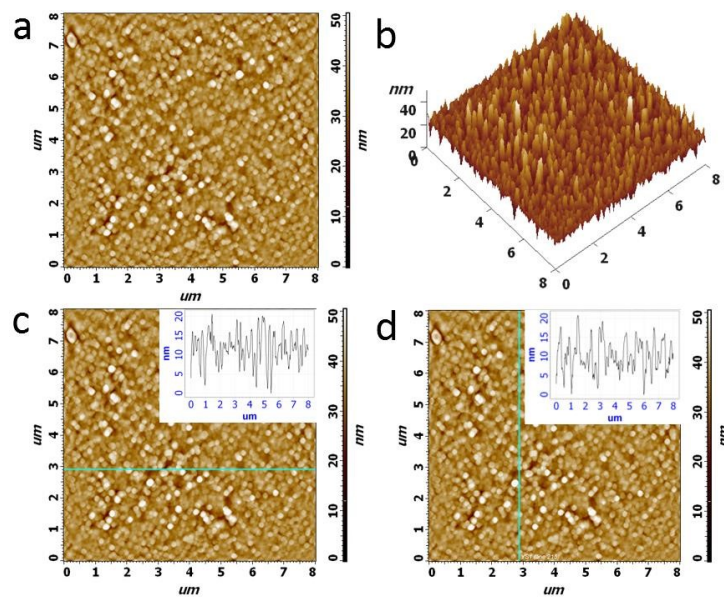


**Figure 4.16** Tapping-mode AFM image of 5-APIn fabricated at optimum pressure (45 mN/m) via LS method (a) 2D (b) 3D (c) and (d) horizontal and vertical surface profile.
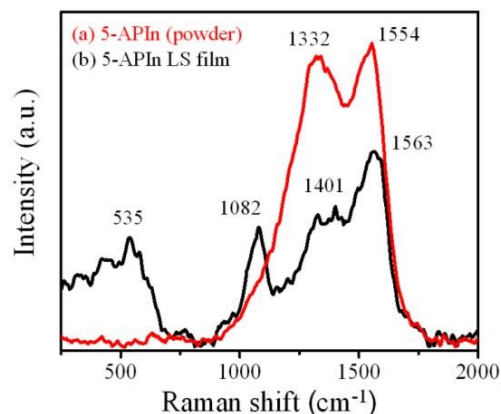
**Figure 4.17** Raman spectra of (a) 5-APIn LS film and (b) 5-APIn powder (bulk).

indicating the improved crystallinity of the LS deposited film [18,55]. The presence of extra peaks for LS film spectrum can be accounted to the better ordering and crystallinity as compared to the bulk polymer due to following two reasons: (1) APIn dispersion prepared in slow evaporating solvent mixture and (2) its spreading over air-water interface allows maximum extension and chain orientation of the molecules over the water subphase. Molecules after slow evaporation of the solvent are suspended at the air-water interface forming floating islands (evident from SEM, Figure 4.15 (a)) on the water subphase. These molecules are suspended probably due to hydrophilic end interacting with water surface and hydrophobic part standing away from the interface.

Pictorial representation shown in Figure 4.18 clearly explains the assembly of 5-APIn chains on water subphase and their arrangement after barrier compression. Amino group present on the chain facilitates this orientation of the molecules in a particular fashion. Further on barrier compression (upto 45 mN/m), these molecules then start coming closer thus interacting with each other and forming a solid compact film. These as-deposited LS films reveal better crystallinity and ordering showing broad and sharp peaks in the Raman spectrum [18,55,76].
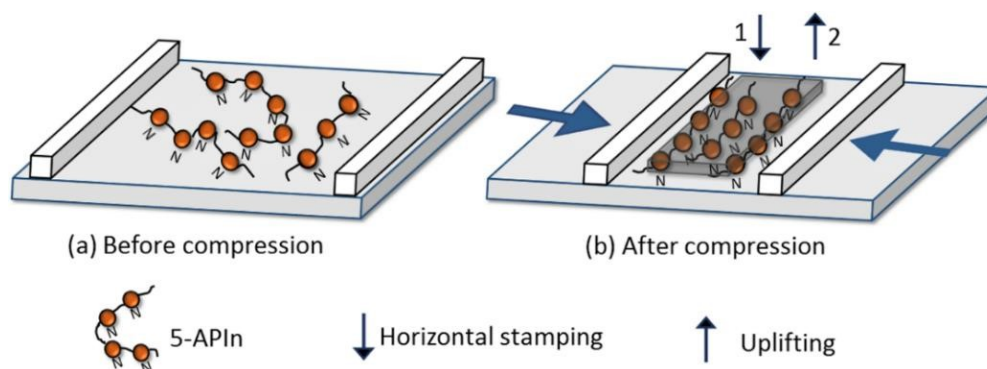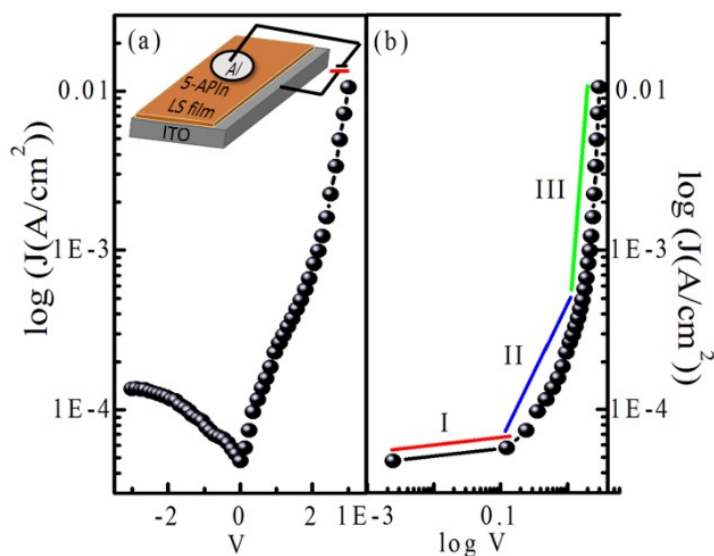
**Figure 4.18** Pictorial representation depicting the 5-APIn dispersion spread over water subphase (a) before and (b) after compression upto 45 mN/m and its LS film fabrication.

## 4.2.9 Electronic parameter and charge transport characteristics

The junction properties of APIn LS film semiconducting polymer, sandwiched between



**Figure 4.19** (a) log J vs. V plot and (b) log J vs. log V plot of sandwiched structure Al/APIn LS film/ITO.

two electrodes totally depend on the interfacial characteristics and the difference in their work function respectively [64,65,100,130]. Therefore, for fabrication of diode, the selected electrodes must be in such a way that one electrode forms ohmic contact with

APIn LS film (p-type semiconductor) and other electrode creates rectifying contact with the semiconducting layer. Therefore, Al and ITO are opted as two electrodes for formation of Schottky diode with the work function of ITO (4.9 eV) comparable with APIn polymer (5.1 eV) forming ohmic contact. Meanwhile, the other electrode Al (4.2 eV) with lower work function forms the rectifying contact.

The current density-voltage (J-V) measurement of device Al/APIn LS Film/ITO was measured by sweeping -3 to +3 V and found asymmetrical rectifying nature in first and third quadrant which authorizes the formation of Schottky junction between the Al metal and P3HT [55,100,130]. The semilog plot of log J vs.V characteristics of device Al/APIn LS film/ITO are shown in Figure 4.19 (a). The linear portion of log J vs. V curve is used to estimate the ideality factor as shown in Figure 4.19 (b). The electrical characteristics of Schottky junction can be explained using standard thermionic emission-diffusion theory [56,63]. As per thermionic emission-diffusion theory, J can be related to V with the expression:

$$J = J_0 \left[ \exp\left(\frac{qV}{\eta kT}\right) - 1 \right] \qquad (4.2)$$

where J and $J_0$ denote current density flowing through the diode, reverse saturation current density; q, V, T, η, k, represent the electronic charge, applied bias voltage, absolute temperature, ideality factor, Boltzmann constant, respectively. Furthermore, $J_0$ is directly connected to barrier height $\phi_B$ as:

$$J_0 = A^*T^2 \exp\left(\frac{-q\phi_B}{KT}\right) \qquad (4.3)$$

where A* denotes effective Richardson coefficient and found to be 120 $Acm^{-2}K^{-2}$. Equation (3) can be approximated as below under forward bias (qV / ηkT >> 1) condition

$$\ln J = \ln J_0 + \frac{qV}{\eta kT} \qquad (4.4)$$

The value of ideality factor for Al/5-APIn LS film/ITO device is evaluated at 300 K from the slop of linear region of J-V characteristics plot as shown in Figure 4.19 (a) and found to be 2.7. The value of ideality factor thus obtained is greater than the standard value (unity), which may account for inhomogeneity present in the film or due to the trap states for the charge carriers [17,18]. The reverse saturation current density was found to be $4.619 \times 10^{-5}$ $\mu A/cm^2$. The barrier height at the interface is calculated from reverse saturation current density $J_0$ and found to be 0.71 eV.

In order to understand the charge transport in sandwiched structure, we have plotted double logarithmic J-V characteristics for Al/5-APIn LS film/ITO structure as shown in Figure 4.19 (b). It is quite obvious that, in forward bias condition, the double logarithmic plot demonstrate three well separated regions assigned as (I) ohmic behavior, (II) trap-filled space charge limited current (SCLC) and (III) trap-free space charge limited current (TFSCLC). It can be observed from double log plot that regions I to III are arranged in ascending order of their slop. In particular, region II has higher slope as compared to region I and can be designated as initiation of abrupt trap filling by injected charge carriers. Furthermore, it is assumed that approximately all the traps are filled at the intersection of II and III regions. However, in region III, the small bias voltage causes the exponential increase in current density. Furthermore, in TFSCLC region, there is only one type of charge carriers either electrons or holes. Al/5-APIn LS film /ITO will be

**Table 4.4** Electronic parameters of Schottky diode configuration.

| Device | $J_0$ (A/cm$^2$) | $\Phi_B$ (eV) | $\eta$ | On/Off ratio |
|---|---|---|---|---|
| Al/APIn LS Film/ITO | $4.619 \times 10^{-5}$ | 0.71 | 2.71 | 120 |

regarded as hole only in region III and electronic parameters of Schottky diode configuration are listed in Table 4.4.

## 4.3    Conclusion

The morphology controlled IP of 5-APIn is achieved successfully in one-pot system yielding electroactive polymer in bulk. This approach provided better asset such as better electrochemical properties (large electrochemical window) than electrochemically synthesized same polymer. Due to protonation of the amino group present at the C-5 position of 5-APIn; 1, 3-linkage in monomers is achieved, ascertained by ^{1}H-NMR and FT-IR techniques. Bathochromic shift is observed due to extension in conjugation length of 5-APIn as compared to its monomer. The presence of amino group resulted in better crystallinity than its unsubstituted analog as evident by the XRD pattern. This template-free technique provided ample of time without disturbance for polymer to acquire its non-uniform globular morphology and porous structure (monitored via SEM). Apart from this, amino group on polymer backbone facilitated good redox quasi-reversibility (both p-and n-type doping property) under applied potentials in nonaqueous medium. However in aqueous medium, protonation of amino group depressed the positive potential (still greater than that for electrochemically prepared 5-APIn) for redox recyclability. These observations related the concept of constant phase element (as discussed in EIS results) with the inhomogeneous charge distribution over polymer matrix. The above properties motivated us to explore the electronic properties computationally as well. DFT calculations using hybrid functionals in gas phase are performed in order to estimate electronic properties and predict reasonable structure of the as-synthesized polymer. Theoretical band gap ($\Delta E$=3.82 eV) are estimated to correlate optical band gap ($E_g$=3.06 eV) and electrochemical band gap (oxidation and reduction potentials, $E_{cv}$=3.07 eV).

These values obtained with above methods may differ substantially for conducting organic polymers. So, the difference of ~0.76 eV can be ignored. The amino group on polymer backbone as well as the synthetic methodology employed have recognized this material to show enormous potential for applications in optical, electrochemical and electronic devices. Moreover, the as-proposed morphology controlled synthesis approach motivated for its large area, ordered, compact film of 5-APIn via LS method. Mobile liquid substrate facilitated the formation of ordered and uniform film over various substrates that were validated via SEM and AFM morphology. Further, SEM analysis of 5-APIn LS films deposited at different surface pressures give an insight to the film uniformity prior to film fabrication for device application. Polymer chain ordering in LS film was justified via Raman studies, depict improved ordered, self-assembled nature as compared to bulk. Charge transport property investigation in sandwiched structure reveals its scope for application in further large area based flexible electronic devices.